# Search for octupole correlations in $^{147}$Nd

E. Ruchowska,[1,*] H. Mach,[1,†] M. Kowal,[1] J. Skalski,[1] W. A. Płóciennik,[1,†] and B. Fogelberg[2]
[1]*National Center for Nuclear Research, Hoża 69, PL 00-681 Warsaw, Poland*
[2]*Department of Nuclear and Particle Physics, Uppsala University, P.O. Box 535, S-75121 Uppsala, Sweden*
(Received 16 March 2015; revised manuscript received 22 July 2015; published 29 September 2015)

Properties of excited states in $^{147}$Nd have been studied with the multispectra and $\gamma\gamma$ coincidence measurements. Twenty-four new $\gamma$ lines and three new levels have been introduced into the level scheme of $^{147}$Nd. Using the advanced time-delayed $\beta\gamma\gamma(t)$ method, we measured lifetimes of eight excited levels in $^{147}$Nd, populated via the $\beta$ decay of $^{147}$Pr. We have determined reduced transition probabilities for 30 $\gamma$ transitions. Multidimensional potential energy surface calculations performed for $^{147}$Nd suggest two single-quasiparticle configurations with nonzero octupole deformation, with $K = 1/2$ and $K = 5/2$. Our calculations also predict a sizable value of the electric dipole moment $|D_0| = 0.26e$ fm for this nucleus, while experimentally, a lower limit of $|D_0| \geqslant 0.02e$ fm has been evaluated for the supposed $K = 1/2$ parity doublet. In contrast to the theoretical results, we do not observe the parity doublet bands with $K = 5/2$. This, and the lack of theoretically expected $E1$ strength in $^{147,149}$Nd may signal some poorly understood structural effect in the odd-$N$ lanthanides.

DOI: 10.1103/PhysRevC.92.034328 PACS number(s): 21.10.Re, 21.10.Tg, 23.20.Lv, 27.60.+j

## I. INTRODUCTION

Low-lying negative parity states with fast $E1$ transitions to the ground-state band and high values of the observed electric dipole moments $|D_0|$ suggest that even-even $^{146-150}$Nd nuclei belong to the octupole-deformed region in lanthanides. Theoretical calculations [1,2] support this picture. Therefore one could expect that the intermediate odd-$N$ neodymium isotopes would exhibit parity doublet bands connected by strong $E1$ transitions with high $|D_0|$ moments, typical for the octupole collectivity in odd-$A$ nuclei. However, it is not so: in $^{149}$ Nd, whose properties have been studied in Ref. [3], small values of $|D_0|$ have been obtained for the lowest opposite parity states, which should constitute a parity doublet. The aim of the present study is to investigate experimentally and theoretically the octupole correlations in the neighboring odd-$A$ $^{147}$Nd.

Excited states in $^{147}$Nd have been studied previously in the $\beta$ decay of $^{147}$Pr [4–6], in the neutron capture reaction [7,8] as well as in transfer reactions [9–12]. Recently, high-spin states in $^{147}$Nd have been studied using heavy-ion induced fusion-fission reactions [13]. Multipolarities of several $\gamma$ transitions in $^{147}$Nd have been established in Refs. [6,8] by internal-conversion electron measurements. Lifetimes of the lowest levels in $^{147}$Nd have been measured in Refs. [6,10]. Experimental data concerning the $^{147}$Nd nucleus are gathered in a recent compilation [14]. Despite a rather big amount of data on $^{147}$Nd, no firm configuration assignment for excited levels was proposed and there is not much experimental information about octupole correlations.

In order to better understand the low energy structure and to obtain new information on the strength of the octupole interactions in $^{147}$Nd we have measured lifetimes of the excited states in this nucleus using the advanced time-delayed $\beta\gamma\gamma(t)$ method [15–17]. The paper is organized as follows: the experimental methods are briefly described in Sec. II while a proposed new level scheme for $^{147}$Nd and the lifetime results are presented in Sec. III. In Sec. IV experimental results are discussed and compared to theoretical calculations: of potential energy surfaces and estimates of $|D_0|$ moments.

## II. EXPERIMENTAL DETAILS

Measurements were carried out at the OSIRIS on-line fission-product mass separator at Studsvik in Sweden [18]. Excited states in $^{147}$Nd were populated in the $\beta$ decay of $^{147}$Pr, which was obtained via a chain of $\beta$ decays starting from the $^{147}$Cs and $^{147}$Ba isotopes,

$$^{147}\mathrm{Cs} \xrightarrow{0.230s} {}^{147}\mathrm{Ba} \xrightarrow{0.894s} {}^{147}\mathrm{La} \xrightarrow{4.06s} {}^{147}\mathrm{Ce} \xrightarrow{56.4s} \rightarrow {}^{147}\mathrm{Pr} \xrightarrow{13.4\mathrm{min}} {}^{147}\mathrm{Nd}.$$

The $A = 147$ nuclei were produced in the fission reaction of $^{235}$U induced by the thermal neutrons from the R2-0 reactor at Studsvik. The $^{235}$U target consisted of about 1 g of uranium dispersed in graphite. The $A = 147$ activity, mass separated from other fission products, was deposited onto an aluminized mylar foil in a moving-tape collection system at the center of the experimental setup. Each measuring cycle was divided into eight sequential time-bins, each lasting 40 s. To 'clean up' spectra from the activities coming from the $^{147}$Pr predecessors, our radioactive samples were cumulated during the first 135 s of each cycle. Then the beam was deflected and the data were collected during the rest of the cycle.

Two experiments have been performed. In the first one, the multispectra (MSS) and $\beta$-gated $\gamma\gamma$ coincidence data have been collected. In this experiment, one LEP Ge detector with energy resolution FWHM of 0.6 keV at 81 keV, one 30% HPGe detector with FWHM of 2.1 keV and one 80% HPGe detector with FWHM of 2.9 keV at 1333 keV have been used. A 3 mm thick NE111A plastic scintillator was used as a $\beta$ detector. About $1.2 \times 10^8$ double coincident events have been collected.

*ewa.ruchowska@ncbj.gov.pl
†Deceased

 

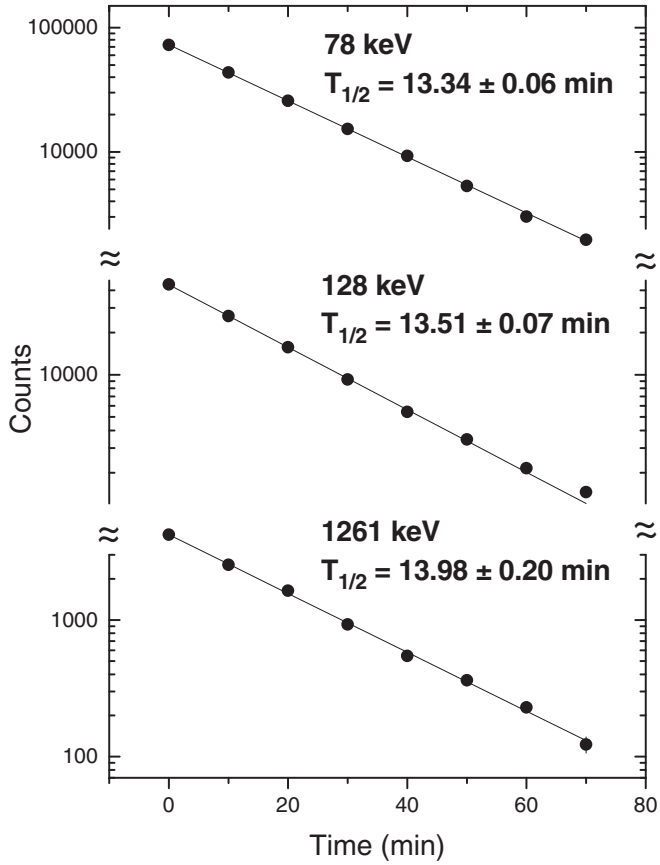


FIG. 1. Examples of the decay curves of $\gamma$ rays from the $\beta$ decay of $^{147}$Pr obtained in the MSS measurements.

In the second experiment, lifetime measurements have been performed using the advanced time-delayed $\beta\gamma\gamma(t)$ method [15–17]. The fast timing information was derived from coincidences between fast-response $\beta$- and $BaF_2$ $\gamma$-detectors, while an additional coincidence with a Ge $\gamma$ detector was used to select the desired $\gamma$ cascade. The setup consisted of one $BaF_2$ detector, one HPGe detector with efficiency of 30% and FWHM of 2.1 keV at 1333 keV, and one $\beta$ detector. The latter was a 3 mm thick $\Delta E$ NE111A plastic detector to ensure almost constant time response of the fast timing system, independent of the $\beta$-particle energy. About $2.2 \times 10^6$ $\beta$-Ge-$BaF_2(t)$ coincident events have been collected. Several sets of the $\beta$-gated coincidence $\gamma$-ray spectra from the Ge and $BaF_2$ detectors and triple coincidence $\beta\gamma\gamma(t)$ time-delayed spectra have been sorted in the off-line analysis. Gating conditions set on the $\beta$ spectrum were chosen to keep the time response constant in the whole range of selected $\beta$-particle energies.

## III. EXPERIMENTAL RESULTS

The results for $^{147}$Nd are presented in Figs. 1–6 and in Tables I and II. Gamma lines were assigned to the $^{147}$Nd level scheme based on the MSS and $\gamma\gamma$ coincidence results. Figure 1 presents examples of the decay curves for $\gamma$ transitions emitted in the $\beta$ decay of $^{147}$Pr obtained in the MSS measurements. The average half-life of $^{147}$Pr obtained from these measurements is equal to 13.39(4) min, in agreement with the value 13.4(3) min given in Ref. [14].

The level scheme was constructed based on the $\beta$-Ge-Ge data. Moreover several lines were placed in the level scheme based on the energy fit. Examples of coincident $\gamma$-ray spectra collected with the Ge detectors are shown in Figs. 2 and 3 (upper panels), while a new level scheme for $^{147}$Nd is presented in Figs. 4–6. Level and $\gamma$-ray energies, and $\gamma$-ray intensities determined in the present work are given in Tables I and II. The $E2/M1$ mixing ratios of $\gamma$ transitions were taken from Ref. [14].

In general, our level scheme for $^{147}$Nd well agrees with that obtained by Shibata *et al.* [6]. Twenty-four new $\gamma$ lines and three new levels at energies 830.0, 1761.9, and 2070.4 keV have been introduced into the decay scheme of $^{147}$Pr. They are marked with asterisks in Figs. 4–6 and in Tables I and II. The latter two levels may correspond to the $1759 \pm 5$ and $2068 \pm 5$ keV states, observed in the transfer reactions [14]. Also the $^{147}$Pr $\beta$-decay data obtained with the total absorption $\gamma$-ray spectrometer [19] indicate existence of states with similar excitation energies in $^{147}$Nd. For completeness, weak transitions which have not been observed in our spectra (mainly due to a limited statistics), but reported in Ref. [14], are drawn with dotted lines in the level scheme.

Level lifetimes were determined from the analysis of the triple coincidence $\beta$-Ge-$BaF_2$ data. First the $\gamma$-ray spectra from the $BaF_2$ detector coincident with the $\gamma$ lines registered in the Ge detector were sorted. Examples of these $BaF_2$ spectra are shown in the lower panels of Figs. 2 and 3. Then the fast timing spectra for $\gamma$ lines selected in the $BaF_2$ spectra were extracted. They show the time distributions for these prompt or delayed $\gamma$ transitions measured relative to the $\beta$ detector.

Lifetimes longer than about 40 ps, which manifest themselves by a strong asymmetry (or slope) on the delayed side of the time spectra, have been determined using the deconvolution method [15]. Examples of such time-delayed spectra for the 127.9, 214.6, and 314.7 keV levels in $^{147}$Nd are shown in Fig. 7. The fitted function includes four free parameters, namely the position and full width at half-maximum of the Gaussian approximating prompt time response of the timing detectors, the half-life value, and, finally, a parameter which provides an overall renormalization between the experimental and fitted time spectra. Details on the fitting procedures are given in Ref. [15]. The half-lives for the levels at 49.9, 127.9, 214.6, 314.7, and 604.5 keV have been determined by the deconvolution method.

Lifetimes shorter than 40 ps were measured using the centroid shift method in which the mean lifetime $\tau = T_{1/2}/\ln 2$ is determined as a shift of the centroid of the time-delayed spectrum from the prompt curve. Details of this method, as well as corrections that must be applied when using it, are given in Refs. [15,17]. The method is based on the concept of a two-$\gamma$-ray cascade, which is used to extract the lifetime of an intermediate level. Setting a gate in the Ge detector on a lower transition in the cascade, below the intermediate state, and in

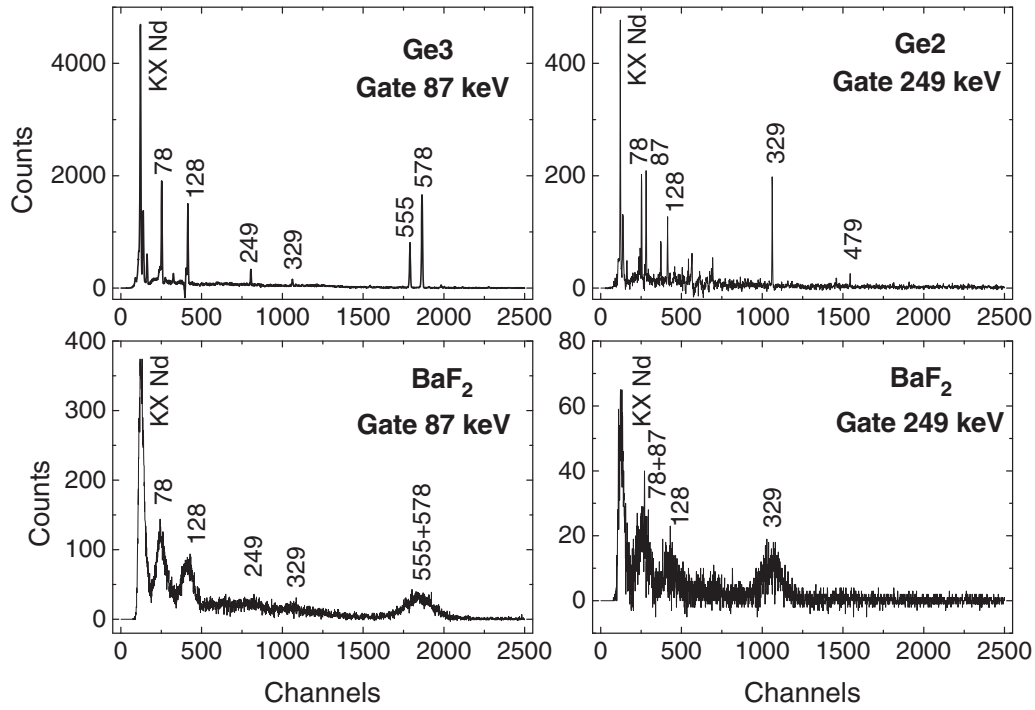


FIG. 2. Coincident $\gamma$-ray spectra from the Ge and $BaF_2$ detectors. Left top panel shows spectrum from the 80% HPGe detector gated by the 86.7 keV line in the LEP detector. Right top panel shows spectrum from the 30% HPGe detector gated by the 249.0 keV line in the LEP detector. Panels at the bottom show the corresponding coincident spectra sorted onto the $BaF_2$ detector from the $\beta$-Ge-$BaF_2$ data.

the $BaF_2$ detector on an upper transition one obtains a position of the first time peak, subsequently used as a reference point. It is shifted from the time peak position of the prompt $\gamma$ ray by the mean lifetime of the higher level. Let us mention here that the lifetime of this particular level, or any higher lying level that feeds it, does not need to be known at all, since they finally cancel out. By reversing gates in the $BaF_2$ and Ge detectors, namely selecting the upper transition in the Ge

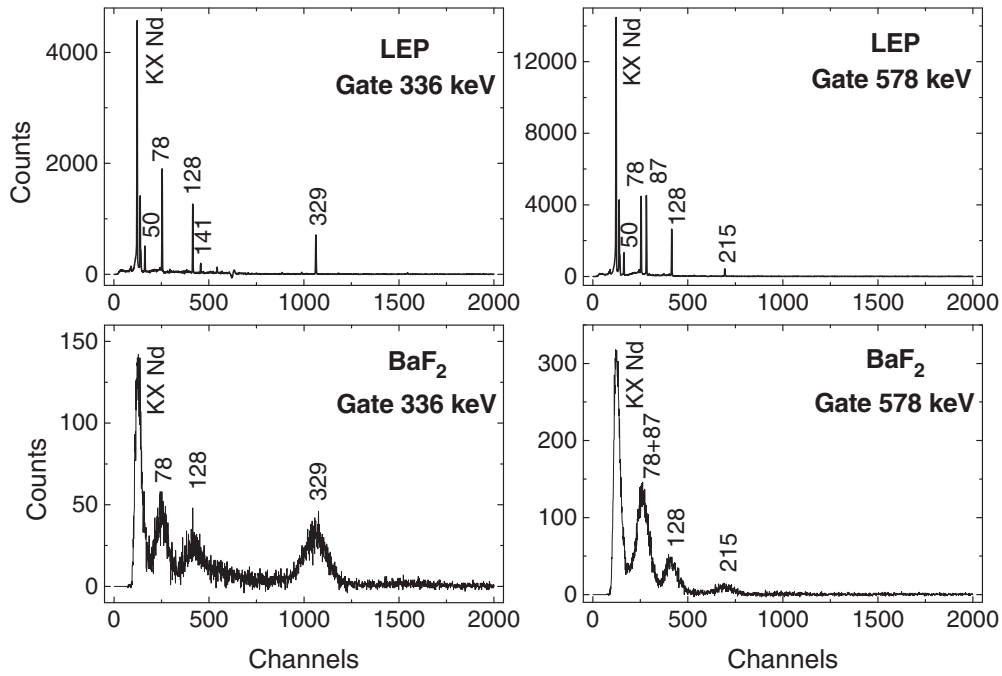


FIG. 3. Coincident $\gamma$-ray spectra from the Ge and $BaF_2$ detectors. Left top panel shows spectrum from the LEP detector gated by the 335.7 keV line in the 30% HPGe detector. Right top panel shows spectrum from the LEP detector gated by the 578.0 keV line in the 80% HPGe detector. Panels at the bottom show the corresponding coincident spectra from the $BaF_2$ detector.

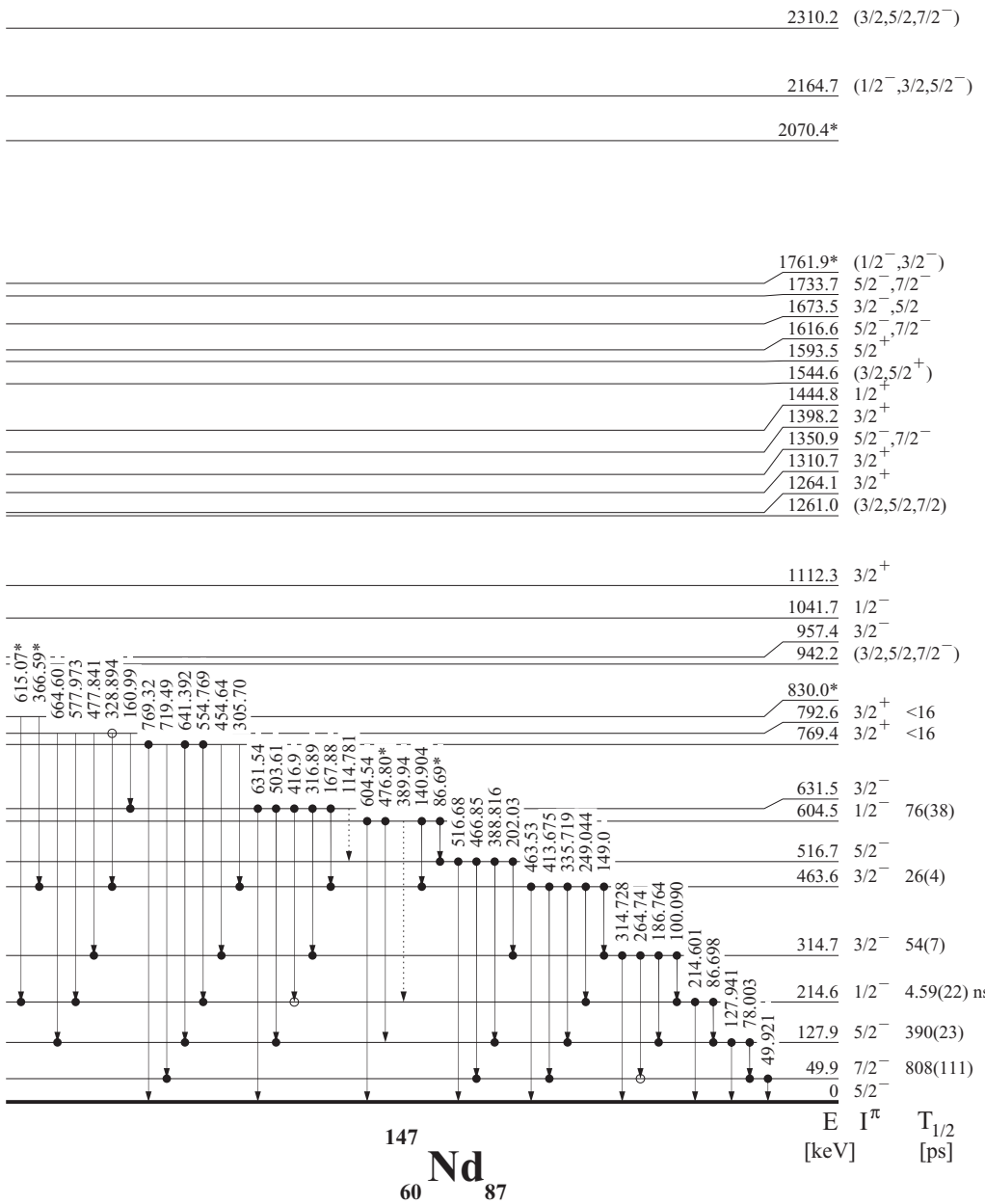


FIG. 4. Part I of the level scheme of $^{147}$Nd from the $\beta$ decay of $^{147}$Pr. Full and empty circles indicate strong and weak $\gamma\gamma$ coincidence relations, respectively. Dotted lines mark transitions reported in Ref. [14] but not observed in our data due to limited statistics. Asterisks indicate new levels and transitions observed in this work in the $\beta$ decay of $^{147}$Pr.

detector and the lower one in the $BaF_2$ crystal, we determine the position of the second time peak. It is shifted from the time peak position of the prompt $\gamma$ ray by the sum of the mean lifetimes of the upper and intermediate level. The difference of these two time peak positions gives the mean lifetime of the intermediate level. However, in real experiment the time peak positions of the prompt $\gamma$ rays depend on their energies. To take this into account one uses the time reference curve which shows the time peak positions of the prompt $\gamma$ transitions versus their energy. By shifting both time peak positions so that the first of them is placed on the time reference curve at the energy of the upper transition, we obtain the mean lifetime of the intermediate level as a distance of the second time peak position from the time reference curve at the energy of the lower transition.

The time reference curve was constructed from the $\beta$-gated $\gamma\gamma(t)$ data measured for the $^{138}$Cs calibration source in the same conditions as in the main experiment. Further details of the centroid shift method can be found, e.g., in Refs. [20–26] where this method has been applied. In this way a half-life of 26(4) ps was obtained for the 463.6 keV level as an average from the time spectra obtained with the 328.9–249.0, 328.9–335.7, 328.9–413.7, and 887.0–335.7 keV Ge-$BaF_2$ gate combinations. Examples of short half-life determination

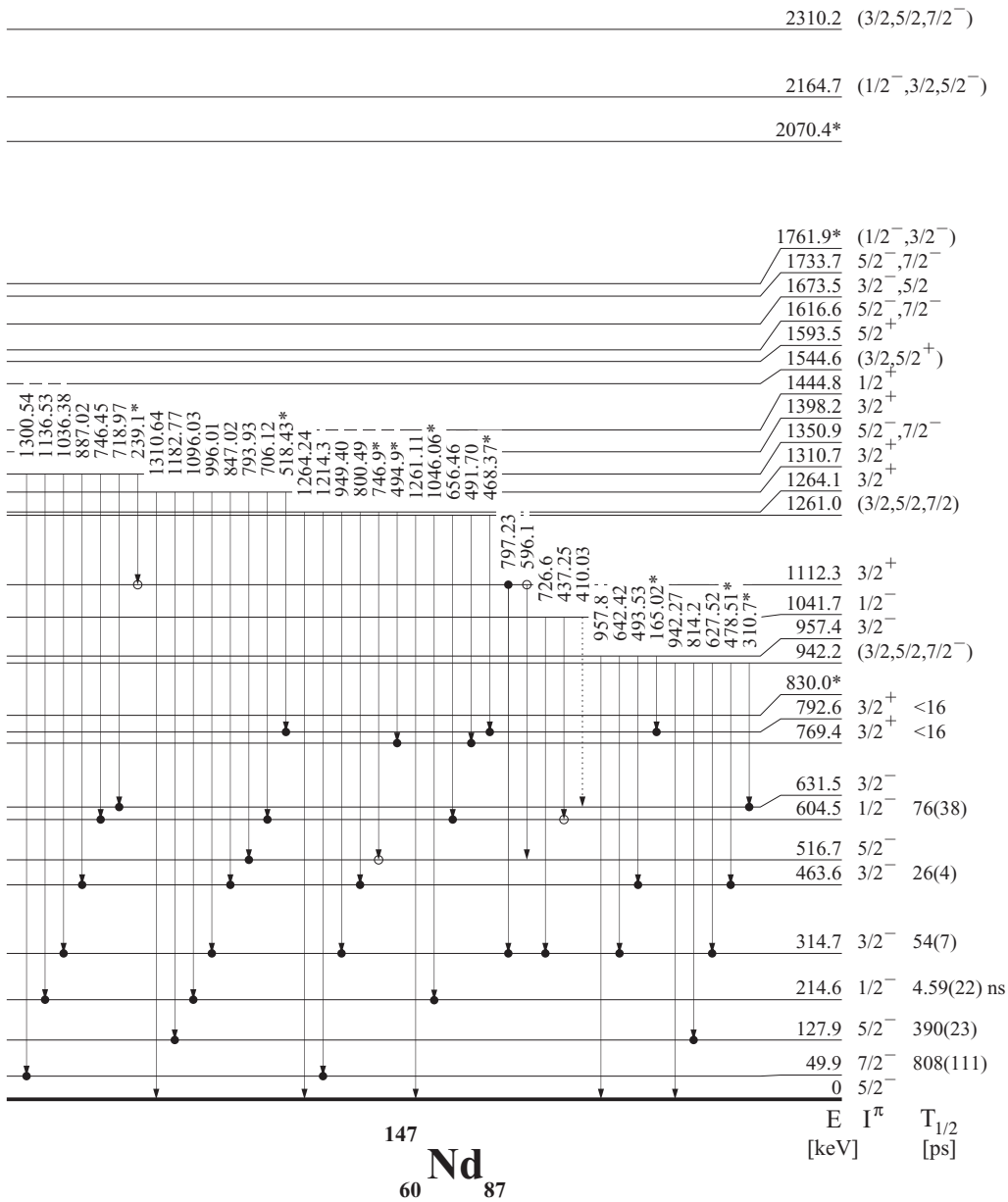


FIG. 5. Part II of the level scheme of $^{147}$Nd from the $\beta$ decay of $^{147}$Pr.

using the centroid shift method are given in Fig. 8. Besides, we have obtained half-life limits for the 769.4 and 792.6 keV levels in $^{147}$Nd.

The half-life values obtained in the present work for excited states in $^{147}$Nd are given on the level scheme and are listed in the third column in Table I. Up to now, only the half-lives for the first three excited states had been determined in $^{147}$Nd [14]. Our half-lives obtained for these levels agree very well with the values given in the cited paper. For next three excited states only nanosecond half-life limits had been previously known (see column 4 of Table I). Here, we have determined their half-lives much more precisely.

Reduced transition probabilities for 30 transitions in $^{147}$Nd, determined in this work, are listed in the last column of Table I. They were deduced from the level lifetimes and the relative $\gamma$-ray intensities, using the total internal conversion coefficients from Ref. [27].

## IV. DISCUSSION

### A. Band structure in $^{147}$Nd

As mentioned in the introduction, strong octupole correlations in odd-$A$ nuclei are mainly manifested by the presence of parity doublet bands, connected by the enhanced $E1$ transitions with the reduced transition probabilities $B(E1)$ of the order of $10^{-3}e^2$ fm$^2$ [2]. In doublet $K^\pi = 1/2^\pm$ bands, one expects the decoupling parameters of opposite sign and equal magnitude.

To provide some theoretical insight, we used the microscopic-macroscopic method based on the deformed

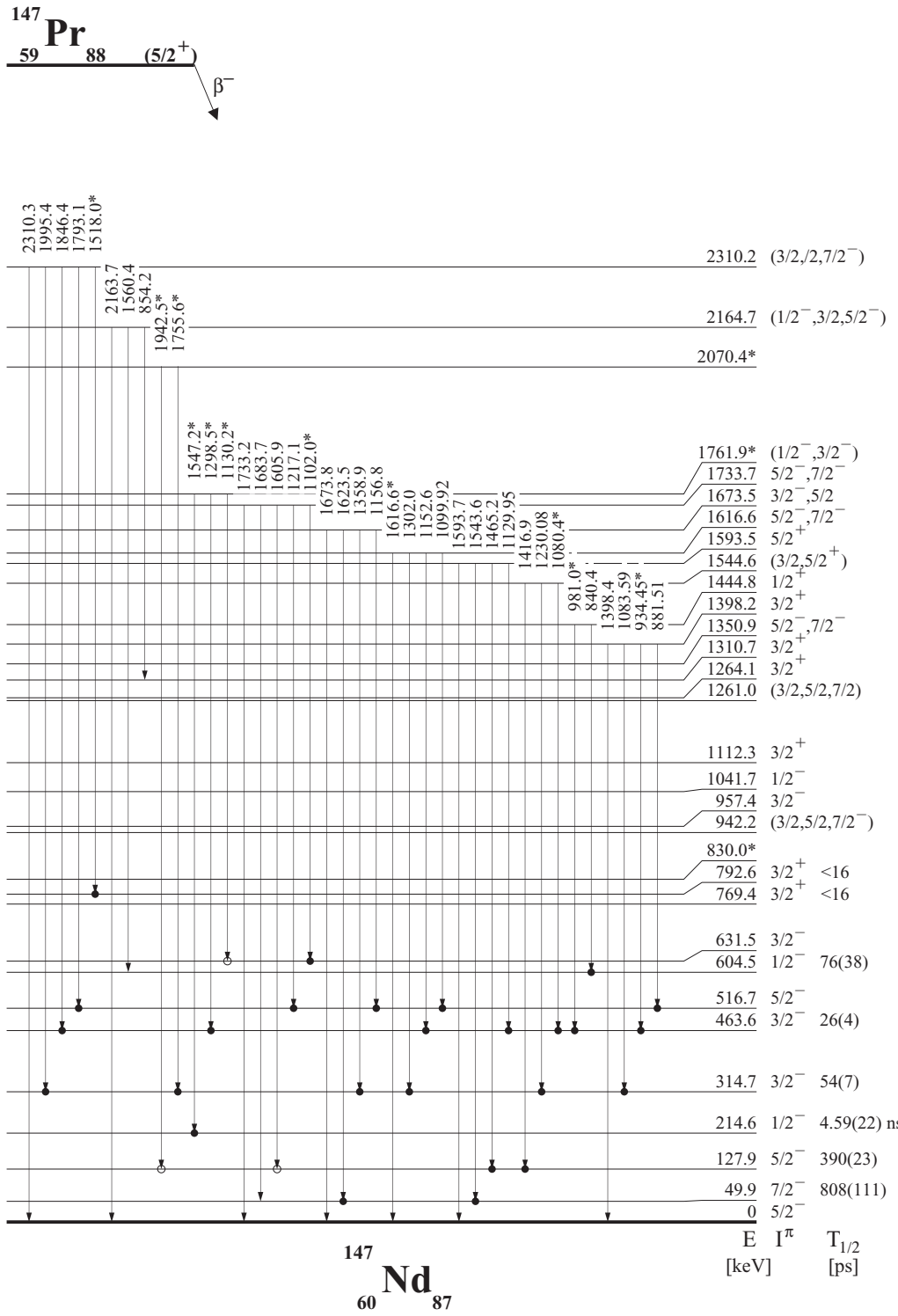


FIG. 6. Part III of the level scheme of $^{147}$Nd from the $\beta$ decay of $^{147}$Pr.

Woods-Saxon potential (see Sec. IV C), previously often applied in studies of octupole collectivity. Multidimensional potential energy surface (PES) calculations have been performed with blocking the lowest-lying quasiparticle states. The model predicts two octupole-soft states with $K = 1/2$ and $K = 3/2$ and two octupole-deformed states with $K = 1/2$ and $K = 5/2$. Thus, we looked for candidates for two parity doublet bands in our data: one with $K^\pi = 1/2^\pm$ and second one with $K^\pi = 5/2^\pm$.

The ground state and the excited $7/2^-$ state at 49.9 keV are candidates for the $K^\pi = 5/2^-$ band, per analogy with $^{149}$Nd [3]. The magnetic factor $|g_K - g_R|$ for this band,

TABLE I. Level lifetimes and experimental reduced transition probabilities in $^{147}$Nd observed in the $\beta$ decay of $^{147}$Pr. New $\gamma$ transitions are marked with an asterisk.

| Initial level [keV] | $I_i^\pi K_i$ | $T_{1/2}$ this work [ps] | $T_{1/2}$ Ref. [14] [ns] | $E_\gamma$ [keV] | $I_\gamma$ | $I_f^\pi K_f$ | $M\lambda$[a] | $\alpha_{TOT}$[b] | $B_{exp}(M\lambda)$[c] |
|---|---|---|---|---|---|---|---|---|---|
| 49.9 | $7/2^-$ 5/2 | 808(111) | 1.0(3) | 49.921(4) | 48(5) | $5/2^-$ 5/2 | $M1$ | 10.5 | $>2.3\times10^{-2}$ |
| | | | | | | | $E2$ | 31.3 | $<2.3\times10^{4}$ |
| 127.9 | $5/2^-$ 1/2 | 390(23) | 0.4(1) | 78.003(5) | 122(12) | $7/2^-$ 5/2 | $M1$ | 2.85 | $>3.0\times10^{-2}$ |
| | | | | | | | $E2$ | 5.4 | $<1.6\times10^{4}$ |
| | | | | 127.941(6) | 100(10) | $5/2^-$ 5/2 | $M1$ | 0.71 | $>5.9\times10^{-3}$ |
| | | | | | | | $(E2)$ | 0.91 | $<8.3\times10^{2}$ |
| 214.6 | $1/2^-$ 1/2 | 4.59(22) ns | 4.53(6) | 86.698(5) | 69(7) | $5/2^-$ 1/2 | $E2$ | 3.9 | $4.8(5)\times10^{3}$ |
| | | | | 214.601(6) | 19(2) | $5/2^-$ 5/2 | $E2$ | 0.155 | $1.4(2)\times10^{1}$ |
| 314.7 | $3/2^-$ 3/2 | 54(7) | $\leqslant$0.1 | 100.090(8) | 5.5(5) | $1/2^-$ 1/2 | $(M1)$ | 1.5 | $1.3(2)\times10^{-2}$ |
| | | | | 186.764(6) | 11.7(12) | $5/2^-$ 1/2 | $M1$ | 0.25 | $4.4(7)\times10^{-3}$ |
| | | | | 264.74(4) | 4.0(4) | $7/2^-$ 5/2 | $E2$ | .082 | $1.1(2)\times10^{2}$ |
| | | | | 314.728(6) | 255(25) | $5/2^-$ 5/2 | $M1$ | 0.06 | $7.4(^{41}_{+38})\times10^{-3}$ |
| | | | | | | | $E2$ | 0.047 | $1.8(^{+7}_{-6})\times10^{3}$ |
| 463.6 | $3/2^-$ 1/2 | 26(4) | $\leqslant$0.1 | 149.0(1) | 0.4(1) | $3/2^-$ 3/2 | $M1$ | 0.46 | $1.8(5)\times10^{-3}$ |
| | | | | 249.044(8) | 15.3(15) | $1/2^-$ 1/2 | $M1$ | 0.112 | $8.8(^{-82}_{+57})\times10^{-3}$ |
| | | | | | | | $E2$ | 0.095 | $1.3(^{+19}_{-13})\times10^{3}$ |
| | | | | 335.719(6) | 67(7) | $5/2^-$ 1/2 | $E2$ | 0.039 | $3.1(6)\times10^{3}$ |
| | | | | | | | $(M1)$ | 0.052 | $1.9(11)\times10^{-3}$ |
| | | | | 413.675(9) | 13.3(13) | $7/2^-$ 5/2 | $E2$ | 0.0208 | $2.3(4)\times10^{2}$ |
| | | | | 463.53(5) | 2.8(3) | $5/2^-$ 5/2 | $M1$ | 0.022 | $4.1(8)\times10^{-4}$ |
| 604.5 | $1/2^-$ 1/2 | 76(38) | <0.8 | 86.69(5)* | 1.6(2)* | $5/2^-$ 3/2 | $(E2)$ | 3.85 | $1.0(5)\times10^{5}$ |
| | | | | 140.904(8) | 3.3(3) | $3/2^-$ 1/2 | $(M1)$ | 0.54 | $2.5(13)\times10^{-2}$ |
| | | | | 389.94(6)[d] | 0.6(2)[d] | $1/2^-$ 1/2 | $(M1)$ | 0.0345 | $2.2(13)\times10^{-4}$ |
| | | | | 476.80(6)* | 1.6(2)* | $5/2^-$ 1/2 | $(E2)$ | 0.0138 | $2.0(10)\times10^{1}$ |
| | | | | 604.54(5) | 9.1(9) | $5/2^-$ 5/2 | $(E2)$ | 0.0075 | $3.5(18)\times10^{1}$ |
| 769.4 | $3/2^+$ 1/2 | $\leqslant$16 | | 305.70(4) | 2.4(2) | $3/2^-$ 1/2 | $(E1)$ | 0.0135 | $\geqslant7.5\times10^{-6}$ |
| | | | | 454.64(5) | 1.4(1) | $3/2^-$ 3/2 | $(E1)$ | 0.005 | $\geqslant1.3\times10^{-6}$ |
| | | | | 554.769(8) | 76(8) | $1/2^-$ 1/2 | $E1$ | 0.00315 | $\geqslant4.0\times10^{-5}$ |
| | | | | 641.392(8) | 215(22) | $5/2^-$ 1/2 | $E1$ | 0.0023 | $\geqslant7.3\times10^{-5}$ |
| | | | | 719.49(7) | 3.8(4) | $7/2^-$ 5/2 | $(M2)$ | 0.0205 | $\geqslant2.1\times10^{2}$ |
| | | | | 769.32(8) | 4.8 (5) | $5/2^-$ 5/2 | $(E1)$ | 0.00155 | $\geqslant9.4\times10^{-7}$ |
| 792.6 | $3/2^+$ | $\leqslant$16 | | 160.99(4) | 1.7(2) | $3/2^-$ | $(E1)$ | 0.072 | $\geqslant3.6\times10^{-5}$ |
| | | | | 328.894(6) | 55(6) | $3/2^-$ 1/2 | $(E1)$ | 0.011 | $\geqslant1.4\times10^{-4}$ |
| | | | | 477.841(8) | 56(7) | $3/2^-$ 3/2 | $E1$ | 0.00435 | $\geqslant4.6\times10^{-5}$ |
| | | | | 577.973(8) | 187(19) | $1/2^-$ 1/2 | $E1$ | 0.00285 | $\geqslant8.7\times10^{-5}$ |
| | | | | 664.60(7) | 3.1(3) | $5/2^-$ 1/2 | $(E1)$ | 0.00215 | $\geqslant9.5\times10^{-7}$ |

[a] $\gamma$-ray multipolarities and $\delta^2$(E2/M1) mixing ratios are taken from Ref. [14].
[b] Total internal conversion coefficients are taken from Ref. [27].
[c] In units $e^2fm^2$ for E1 transitions, $e^2fm^4$ for E2 transitions, $\mu_N^2$ for M1 transitions and $\mu_N^2 fm^2$ for M2 transitions.
[d] $\gamma$-ray energy is from Ref. [14]. $\gamma$-ray intensity is re-calibrated from data of Ref. [14].

deduced from the $B(M1)$ value of the 49.9 keV transition treated as a pure $M1$, would be 0.33(2)—very close to 0.40(2) obtained in $^{149}$Nd.

The $B(E1)$ branching ratios for pairs of 554.8 and 305.7, 641.4, and 305.7, and 641.4 and 544.8 keV transitions de-exciting the 769.4 keV level to the 127.9, 214.6, and 463.6 keV states are equal to 5.3(7), 9.7(13), and 1.8(3), respectively. These values agree very well with the theoretical branching ratios of 5.0, 9.0, and 1.8, calculated with the Alaga rule [28], assuming $K = 1/2$ for all four states. We suggest that the 127.9, 214.6, and 463.6 keV states form the $K^\pi = 1/2^-$ band in $^{147}$Nd, with the parameter $E_0 = 285.7$ keV, the rotational parameter $A = 7.93$ keV and the decoupling parameter $a = 9.47$. The quadrupole moment $Q_0$ for this band, calculated from the reduced transition probability for the 86.7 keV line given in Table I, equals 284(16)$e$ fm$^2$.

The $B(M1)$ branching ratio for the 186.8 and 100.1 keV transitions (see Table I) de-exciting the 314.7 keV level to the $I = 5/2$ and $I = 1/2$ states of the $K^\pi = 1/2^-$ band, equals 0.33(8). This agrees with a theoretical value of 0.20, obtained when K=3/2 is assumed for the 314.7 keV level. The $B(E1)$ branching ratio for the 797.2 and 596.1 keV transitions de-exciting the 1112.3 keV level to the 314.7 and 516.7 keV states equals 1.4(3). This agrees with a theoretical value 1.5, obtained

TABLE II. Energies and intensities of $\gamma$ lines in $^{147}$Nd not listed in Table I. New $\gamma$ transitions and new levels are marked with asterisks.

| $E_\gamma$ [keV] | $I_\gamma$ | Initial level [keV] | $E_\gamma$ [keV] | $I_\gamma$ | Initial level [keV] |
|---|---|---|---|---|---|
| 165.02(4)* | 1.5(2)* | 957.4 | 1036.38(8) | 1.9(2) | 1350.9 |
| 167.88(4) | 2.1(2) | 631.5 | 1046.06(8)* | 1.8(2)* | 1261.0 |
| 202.03(4) | 1.6(2) | 516.7 | 1080.4(1)* | 1.1(1)* | 1544.6 |
| 239.1(1)* | 0.6(1)* | 1350.9 | 1083.59(7) | 10.6(10) | 1398.2 |
| 310.7(1)* | 0.7(1)* | 942.2 | 1096.03(8) | 3.2(3) | 1310.7 |
| 316.89(5) | 1.2(1) | 631.5 | 1099.92(9) | 2.9(3) | 1616.6 |
| 366.59(5)* | 1.6(2)* | 830.0* | 1102.0(1)* | 1.3(1)* | 1733.7 |
| 388.816(8) | 18(2) | 516.7 | 1129.95(9) | 2.5(3) | 1593.5 |
| 416.9(1) | 0.9(1) | 631.5 | 1130.2(2)* | 0.6(1)* | 1761.9* |
| 437.25(5) | 1.6(2) | 1041.7 | 1136.53(7) | 19(2) | 1350.9 |
| 466.85(3) | 18(2) | 516.7 | 1152.6(1) | 2.3(2) | 1616.6 |
| 468.37(5)* | 1.9(2)* | 1261.0 | 1156.8(1) | 1.5(1) | 1673.5 |
| 478.51(8)* | 3.8(4)* | 942.2 | 1182.77(8) | 14.0(14) | 1310.7 |
| 491.70(5) | 4.8(5) | 1261.0 | 1214.3(1) | 4.2(4) | 1264.1 |
| 493.53(7) | 1.1(1) | 957.4 | 1217.1(1) | 2.0(2) | 1733.7 |
| 494.9(1)* | 0.7(1)* | 1264.1 | 1230.08(9) | 2.2(2) | 1544.6 |
| 503.61(5) | 4.8(5) | 631.5 | 1261.11(9) | 54(5) | 1261.0 |
| 516.68(3) | 15(1) | 516.7 | 1264.24(9) | 15.3(15) | 1264.1 |
| 518.43(8)* | 1.0(1)* | 1310.7 | 1298.5(1)* | 1.3(2)* | 1761.9* |
| 596.1(2) | 0.6(1) | 1112.3 | 1300.54(9) | 29(3) | 1350.9 |
| 615.07(6)* | 4.8(5)* | 830.0* | 1302.0(1) | 2.9(3) | 1616.6 |
| 627.52(8) | 4.4(4) | 942.2 | 1310.64(9) | 7.1(7) | 1310.7 |
| 631.54(5) | 9.7(10) | 631.5 | 1358.9(1) | 2.6(3) | 1673.5 |
| 642.42(8) | 1.2(1) | 957.4 | 1398.4(2) | 1.4(3) | 1398.2 |
| 656.46(7) | 2.3(2) | 1261.0 | 1416.9(1) | 2.7(3) | 1544.6 |
| 706.12(7) | 6.9(7) | 1310.7 | 1465.2 (1) | 1.6(2) | 1593.5 |
| 718.97(7) | 4.7(5) | 1350.9 | 1518.0(2)* | 1.6 (2)* | 2310.2 |
| 726.6(1) | 0.6(1) | 1041.7 | 1543.6(1) | 3.0(3) | 1593.5 |
| 746.45(7) | 3.6(4) | 1350.9 | 1547.2(1)* | 2.3(2)* | 1761.9* |
| 746.9(1)* | 1.3(1)* | 1264.1 | 1560.4(2) | 0.8(2) | 2164.7 |
| 793.93(5) | 17.8(1.8) | 1310.7 | 1593.7(1) | 2.5(3) | 1593.5 |
| 797.23(8) | 2.0(2) | 1112.3 | 1605.9(1) | 1.1(1) | 1733.7 |
| 800.49(8) | 2.3(2) | 1264.1 | 1616.6(2)* | 0.9(2)* | 1616.6 |
| 814.2(1) | 1.3(1) | 942.2 | 1623.5(1) | 3.4(3) | 1673.5 |
| 840.4(1) | 1.1(1) | 1444.8 | 1673.8(2) | 1.8(2) | 1673.5 |
| 847.02(8) | 3.0(3) | 1310.7 | 1683.7(2) | 1.6(3) | 1733.7 |
| 854.2(2) | 1.4(3) | 2164.1 | 1733.2(2) | 2.3(3) | 1733.7 |
| 881.51(8) | 4.6(5) | 1398.2 | 1755.6(2)* | 0.5(1)* | 2070.4* |
| 887.02(8) | 6.5(6) | 1350.9 | 1793.1(2) | 2.7(3) | 2310.2 |
| 934.45(9)* | 1.2(1)* | 1398.2 | 1846.4(3) | 0.6(1) | 2310.2 |
| 942.27(8) | 12.3(1.2) | 942.2 | 1942.5(2)* | 1.2(1)* | 2070.4* |
| 949.40(9) | 2.1(2) | 1264.1 | 1995.4(2) | 1.6(2) | 2310.2 |
| 957.8(2) | 1.3(1) | 957.4 | 2163.7(3) | 1.4(3) | 2164.7 |
| 981.0(1)* | 1.1(1)* | 1444.8 | 2310.3(4) | 0.9(2) | 2310.2 |
| 996.01(6) | 20(2) | 1310.7 | | | |

assuming that all three states have $K = 3/2$. Similar situation occurs for the 1083.6 and 881.5 keV transitions de-exciting the 1398.2 keV level, for which we obtain 1.2(2) and 1.5 for experimental and theoretical values, respectively. Next $B(E1)$ branching ratio for the 949.4 and 746.9 keV transitions de-exciting the 1264.1 keV level to the 314.7 and 516.7 keV states, equals 0.8(1) which agrees with a theoretical value of 0.7 when one assumes that the 1264.1 keV level has $K^\pi = 1/2^+$,

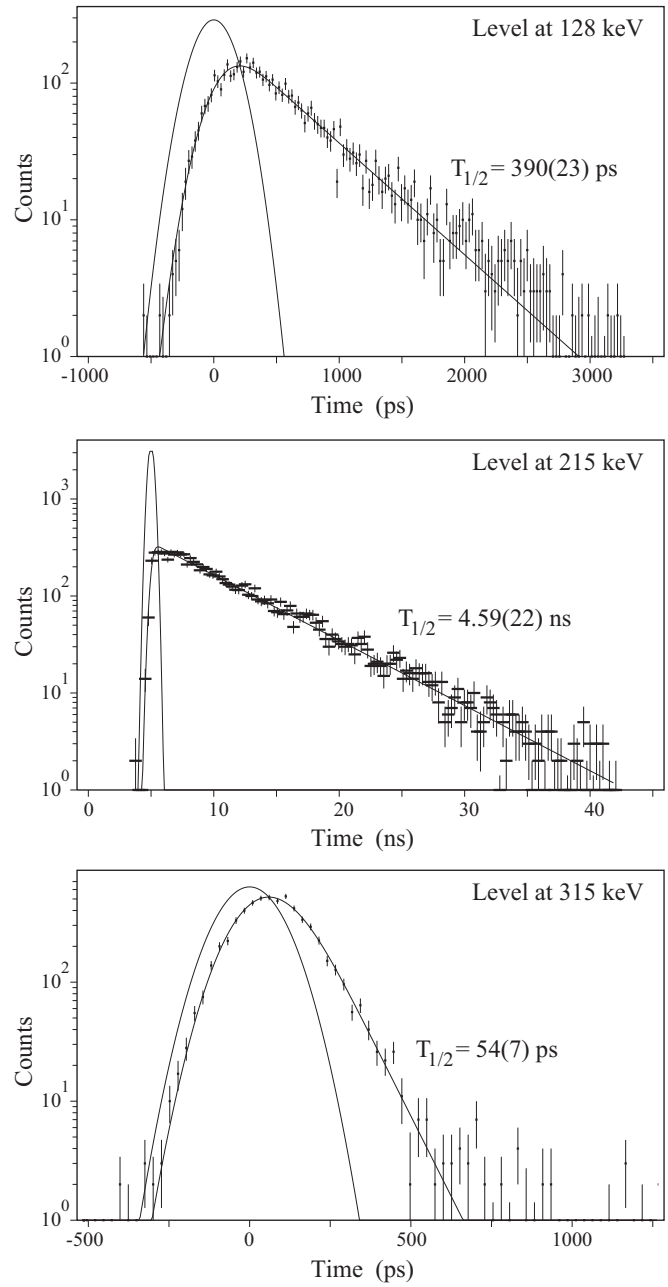


FIG. 7. Time-delayed $\beta\gamma\gamma(t)$ spectra showing slopes due to the lifetimes of the 127.9, 214.6, and 314.7 keV levels in $^{147}$Nd. Each figure shows experimental points, prompt Gaussian spectrum and slope curve, which was fitted in the deconvolution process.

while the 314.7 and 516.7 keV states have $K^\pi = 3/2^-$. All above branching ratios indicate that the 314.7 and 516.7 keV states constitute a band with $K^\pi = 3/2^-$. The proposed band structure for $^{147}$Nd is shown in Fig. 9.

### B. Octupole correlations in $^{147}$Nd

It is significant that we do not observe the $K^\pi = 5/2^+$ band at the lowest excitation energies in $^{147}$Nd, although its population should be enhanced due to the $5/2^+$ ground state spin of the mother nucleus. Neither do we see the $K^\pi = 1/2^+$

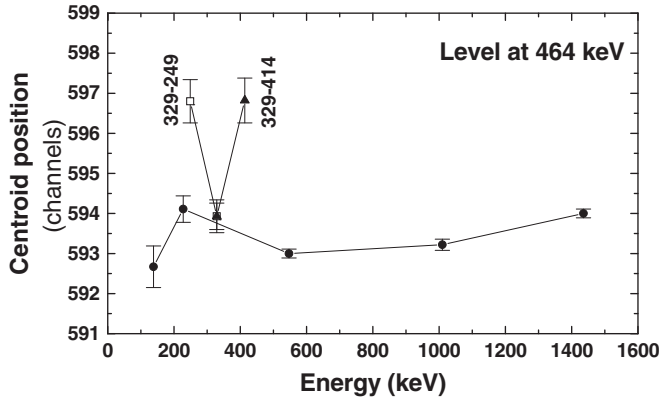


FIG. 8. Determination of the half-life for the 463.6 keV level in $^{147}$Nd by centroid shift technique. The prompt time reference curve (solid circles) made for the $^{138}$Cs calibration source is shown together with the centroid positions of two time-delayed spectra marked by the energies (in keV) of $\gamma$-ray gates in the Ge and $BaF_2$ detectors which were used to generate them: 329–249 (empty squares) and 329–414 (full triangles). The shift of the time-delayed centroid from the prompt reference curve gives the mean-life of the level (calibration 12.85 ps/ch); see text for details.

band close to the $^{147}$Nd ground state. The lowest excited states with opposite parity that could be candidates for the parity doublet members are the $I^\pi K = 3/2^+1/2$ 769.4 keV and the $I^\pi = 3/2^+$ 792.6 keV levels. We were able to determine only the upper limits of their half-lives, $T_{1/2} \leqslant 16$ ps, for both of them. The lower limits of the $B(E1)$ values for the $\gamma$ transitions depopulating these two levels are given in Table I.

As the spin dependence affecting the $B(E1)$ rates is removed in the intrinsic electric dipole moment $|D_0|$, this

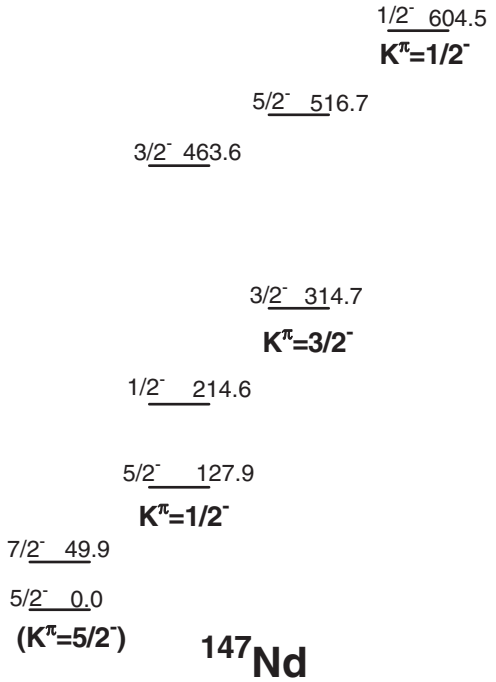


FIG. 9. Interpretation of the band structure in $^{147}$Nd.

quantity allows to compare the $E1$ strength over a wider range of nuclei. By assuming a strong-coupling limit and an axial shape of the nucleus, the electric dipole moment, $|D_0|$, is defined (for $K \neq 1/2$) via the rotational formula:

$$B(E1) = \frac{3}{4\pi} D_0^2 \langle I_i K 10 | I_f K \rangle^2. \quad (1)$$

The $|D_0|$ moment is used as a convenient parameter for the intercomparison even for transitional nuclei.

The lower limit of $|D_0|$ obtained for transitions de-exciting the level at 769.4 keV in $^{147}$Nd to the 127.9, 214.6, and 463.6 keV states from the lower $K^\pi = 1/2^-$ band is $|D_0| \geqslant 0.02e$ fm. If the 792.6 keV level has $K = 1/2$, the lower limit of $|D_0|$ for the 328.9, 578.0, and 664.6 keV de-exciting transitions to the lower $K^\pi = 1/2^-$ band is $|D_0| \geqslant 0.04e$ fm; if it has $K = 3/2$, the limit is $|D_0| \geqslant 0.02e$ fm for the 477.8 keV transition to the $K^\pi = 3/2^-$ band.

Although in $^{147}$Nd we were able to determine only the lower limit of $|D_0|$ for the $K = 1/2$ parity doublet band, the nonobservation of the $K = 5/2$ parity doublet suggests low $|D_0|$ value also for the $K = 1/2$ configuration. A value of $|D_0|$ much lower than in the even-even Nd neighbors has been also found in $^{149}$Nd [3] (see also Table III). The observed variability of $|D_0|$ with neutron number $N$ differs from the smooth dependence known in thorium isotopes from the actinide octupole region (see Fig. 10 in Ref. [3]). It differs also from the theoretically predicted values, see Sec. IV D and Table III there. Moreover, our calculations show that low $|D_0|$ values in the odd-$N$ Nd isotopes cannot result from a quenching caused by opposite signs of the macroscopic and shell-correction components of the dipole moment.

The experimental information on $|D_0|$ moments in the odd-$N$ isotopes in lanthanides is very scarce. Reported $|D_0|$ values are either very low (e.g., in $^{149}$Ce [29]) or no parity doublet bands are found at all. No candidates for parity doublets have been found at the lowest excitation energies in the odd-$N$ barium isotopes: $^{145}$Ba [30] and $^{147}$Ba [31], in spite of the fact that they lie at the very center of the octupole region in lanthanides. Even the ground state spins of these two isotopes can be reproduced without involving octupole correlations [30,31].

Recently, new high-spin data have been reported for the $^{147}$Ce nucleus in Ref. [32]. The $|D_0|$ moments calculated from the $B(E1)/B(E2)$ values given in this reference are 0.18(1) and 0.21(2) $e$ fm for the $31/2^-$, 2703.1 keV and $35/2^-$, 3264.0 keV levels, respectively. These values are comparable to the average $|D_0|$ values of 0.19(3) and 0.21(2) $e$ fm obtained from the $B(E1)/B(E2)$ ratios in the neighboring $^{146}$Ce [33] and $^{148}$Ce [34] isotopes.

It is possible that the considered opposite parity states in $^{147,149}$Nd and in $^{149}$Ce may not constitute parity doublets and the main octupole strength is located at higher excitation energies. More experimental information on the parity doublets and the dipole moments in $^{147}$Nd and other odd-$N$ isotopes in lanthanides are necessary to resolve this issue.

### C. Potential energy surfaces

In order to find equilibrium shapes, we calculated PES for the lowest single-particle configurations in $^{147}$Nd by

TABLE III. Experimental and theoretical $|D_0|$ values in Nd isotopes (in $e$ fm).

| $N$ | 84 | 85 | 86 | 87 | 88 | 89 | 90 |
|---|---|---|---|---|---|---|---|
| Isotope | $^{144}$Nd | $^{145}$Nd | $^{146}$Nd | $^{147}$Nd | $^{148}$Nd | $^{149}$Nd | $^{150}$Nd |
| Experiment | 0.12(1)[a] | | 0.16(4)[b] | $\geqslant$0.02[c] | 0.21(4)[b] | 0.06(2)[d] | 0.26(5)[b] |
| Theory[c] | | 0.15 | 0.17 | 0.26 | 0.30 | 0.36 | |

[a]Determined from level lifetime data given in the www.nndc.bnl.gov data base.
[b]From Ref. [2].
[c]From this work.
[d]From Ref. [3].

using multidimensional macroscopic-microscopic method. Macroscopic energy was calculated using the Yukawa plus exponential model [35] with parameters specified in Ref. [36]. A deformed Woods-Saxon potential [37] with the universal set of parameters [38] was used to calculate the microscopic energy.

Admitted deformations included axially symmetric even-multipole deformations: $\beta_{20}$, $\beta_{40}$,$\beta_{60}$, $\beta_{80}$ and axial odd-multipole deformations: $\beta_{30}$,$\beta_{50}$,$\beta_{70}$. The explicit equation for nuclear radius reads

$$R(\theta) = R_0 c(\{\beta\})\left\{1 + \sum_{\lambda=2}^{8} \beta_{\lambda 0} Y_{\lambda 0}(\theta)\right\}, \tag{2}$$

where $R(\theta)$ is the nuclear radius and $c(\{\beta\})$ is the factor used to impose volume conservation.

We considered single-particle configurations of $^{147}$Nd obtained by blocking the odd neutron on a desired single-particle state with a given $K$. As usual, the Strutinsky shell correction for odd $N$ was calculated with a single occupation of the chosen level. The corresponding pairing correction was obtained for $N-1$ particles, with the blocked level excluded from the spectrum (for a more detailed description see, e.g., [39]). Energies were calculated on a grid of 1 361 367 points defined by deformation values:

$$\begin{aligned}
\beta_{20} &= 0.00\ (0.05)\ 0.30;\\
\beta_{30} &= 0.00\ (0.05)\ 0.30;\\
\beta_{40} &= -0.20\ (0.05)\ 0.20;\\
\beta_{50} &= -0.20\ (0.05)\ 0.20;\\
\beta_{60} &= -0.15\ (0.05)\ 0.15;\\
\beta_{70} &= -0.15\ (0.05)\ 0.15;\\
\beta_{80} &= -0.15\ (0.05)\ 0.15;
\end{aligned} \tag{3}$$

where the step in each deformation is given in parentheses. The most important among odd multipoles is $\beta_{30}$. This is why we show the results from full seven-dimensional grid calculation by projecting them on the $(\beta_{20},\beta_{30})$ plane. For each $(\beta_{20},\beta_{30})$ pair the energy was minimized with respect to the remaining degrees of freedom $\beta_{40} - \beta_{80}$. Energy surfaces obtained for four single-particle configurations in $^{147}$Nd are presented in Fig. 10. They show equilibrium deformations: $\beta_{20}$ of 0.13–0.18 and $\beta_{30} \approx 0.10$. Two configurations, $K = 1/2$ and $3/2$ (energy levels no. 42 and 43) with shallow octupole minima may be called octupole-soft. Slightly more pronounced, $\approx$0.5 MeV deep, octupole minima were obtained for configurations with $K = 1/2$ and $5/2$ (levels no. 44 and 45; the Fermi level in $^{147}$Nd lies in-between levels no. 43 and 44).

Energy calculations for two even-$A$ neighbors of $^{147}$Nd show octupole minima for both $^{146}$Nd and $^{148}$Nd ground states. Thus, our calculations suggest that $^{147}$Nd lies inside the lanthanide octupole collective region.

### D. Theoretical electric dipole moments

Reduced probabilities of electromagnetic (EM) transitions between the rotational band built on the one-octupole-phonon state and the g.s. band can be calculated assuming the fixed structure of both the phonon and the collective rotor [40]. For an operator $\mathcal{M}$ of the multipolarity $\lambda$ one has in odd-$A$ nucleus

$$\begin{aligned}
B(\lambda; K_1, I_1 \to K_2, I_2) = {} & 2\langle I_1 K_1 \lambda K_2 - K_1 | I_2 K_2\rangle^2 \\
& \times |\langle K_2 | \mathcal{M}(\lambda, K_2 - K_1) | K_1\rangle|^2
\end{aligned} \tag{4}$$

with $\mathcal{M}(\lambda,\nu)$ the intrinsic spherical component. For dipole transitions between the pear-shaped parity-doublet bands $\mathcal{M}(E1,0) = [3/(4\pi)]^{1/2}\hat{D}_z$, where the dipole moment $\hat{\mathbf{D}} = e(N\sum_p \mathbf{r}_p - Z\sum_n \mathbf{r}_n)/A$.

In the strong coupling limit, with two deep octupole minima at $\pm\beta_{30}^{eq}$, the transition matrix element $D^t$ is calculated as the intrinsic dipole moment at this deformation of equilibrium. In this case, both the ground-state and the octupole one-phonon state are nearly degenerate and have nearly the same deformation. The results in Table III follow from this way of proceeding. For shallow minima, closer to the oscillation scenario, the degeneracy between parity-doublet bands is shifted. The intrinsic transition matrix element between the g.s. and the lowest excited state of negative parity may be approximated by a diagonal matrix element of the transition operator in the mean-field state with a deformation $\beta_{30}^{tr}$ intermediate between the ground state and the one-phonon state. This would slightly reduce $|D_0|$ as compared to the values presented in Table III (for a more detailed discussion, including a coupling to vibrations of higher odd multipoles, see [41]).

We calculated expectation values of the electric dipole moment in the intrinsic states as a sum of the macroscopic and shell-correction parts, see, e.g., [1,42]. The macroscopic part, derived within the droplet model in Ref. [43], was calculated as in Ref. [44], i.e., without assuming small deformations $\beta_{\lambda 0}$. It turns out (Table III) that intrinsic dipole moments at equilibrium deformations for two configurations: $K = 1/2$

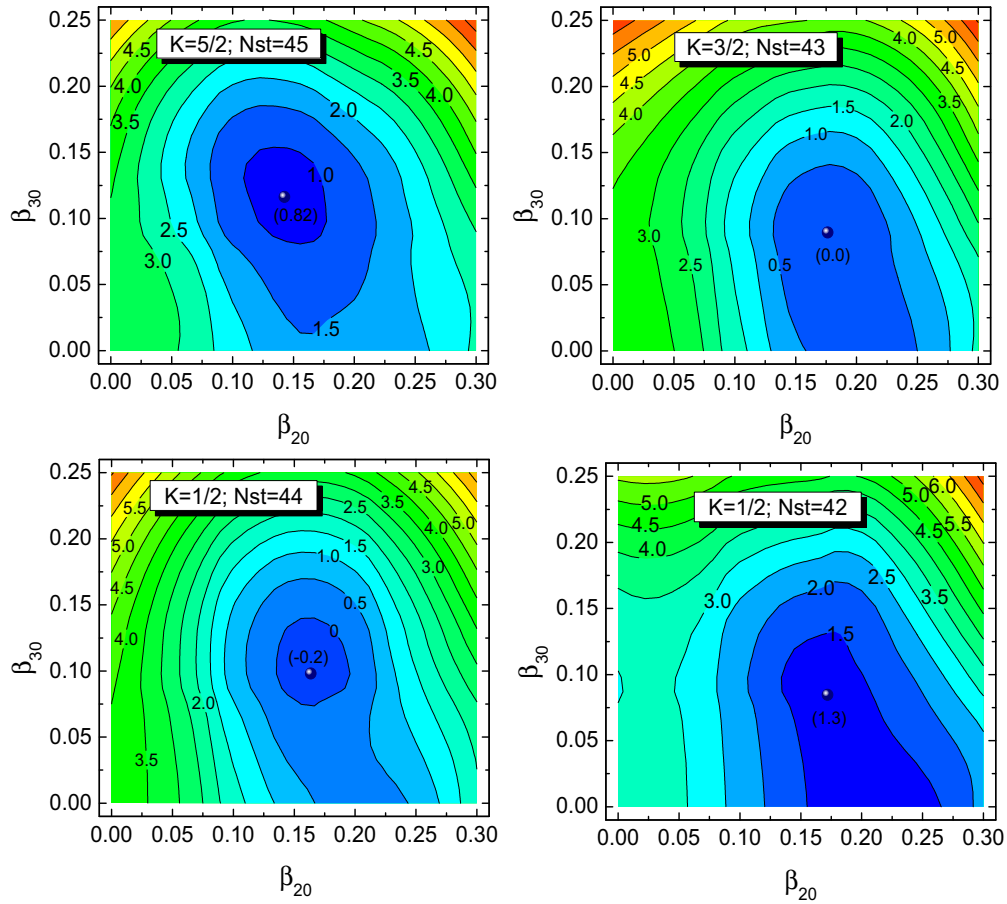


FIG. 10. (Color online) Potential energy surfaces calculated for the lowest single quasiparticle configurations in $^{147}$Nd with $K = 1/2$, $3/2$, and $5/2$ and single particle state numbers $Nst = 42$, 43, 44, and 45. The energy distance between the contour lines is equal to 0.5 MeV.

and 3/2 (levels no. 43 and 44) interpolate the values for $^{146,148}$Nd. Both macroscopic and shell correction contributions have the same sign, so no reduction of $D_0$ due to their cancellation is possible. Thus, the dipole moments inferred from experiment do not fit the picture of parity doublet bands.

## V. SUMMARY

The advanced time-delayed $\beta\gamma\gamma(t)$ method has been used to measure half-lives of eight excited states in $^{147}$Nd. Reduced transition probabilities were obtained for 30 transitions. Twenty-four new $\gamma$ lines and three new levels have been introduced into the level scheme of $^{147}$Nd based on the results of the $\beta$-gated $\gamma\gamma$ coincidence measurement.

The potential energy surfaces on the ($\beta_2$,$\beta_3$) plane and theoretical $|D_0|$ values suggest the presence of octupole deformation in $^{147}$Nd at low excitation energies for two configurations with $K = 1/2$ and $K = 5/2$. This suggestion is supported by high experimental $|D_0|$ values in two even-even neighbors of $^{147}$Nd. For the $K = 1/2$ configuration we were able to determine only the lower limit of the dipole moment, $|D_0| \geqslant 0.02e$ fm. However, the non-observation of the $K = 5/2$ parity doublet band in $^{147}$Nd and low $|D_0|$ values observed earlier in $^{149}$Nd are in contradiction with theoretical predictions. More experimental and theoretical studies are needed to understand the behavior of octupole correlations at low excitations in the odd-$N$ nuclei in lanthanides.

## ACKNOWLEDGMENTS

M.K. and J.S. were co-financed by the National Science Centre under Contract No. UMO-2013/08/M/ST2/0025 (LEA-COPIGAL).

[1] P. A. Butler and W. Nazarewicz, Nucl. Phys. A **533**, 249 (1991).
[2] P. A. Butler and W. Nazarewicz, Rev. Mod. Phys. **68**, 349 (1996).
[3] E. Ruchowska, W. A. Płóciennik, H. Mach, K. Gulda, B. Fogelberg, H. Gausemel, L. M. Fraile, W. Kurcewicz, K. Mezilev, and M. Sanchez-Vega, Eur. Phys. J. A **45**, 1 (2010).
[4] M. Dorikens and L. Dorikens-Vanpraet, Z. Phys. A **275**, 375 (1975).
[5] J. A. Pinston, R. Roussille, G. Bailleul, J. Blachot, J. P. Bocquet, E. Monnand, B. Pfeiffer, H. Schrader, and F. Shussler, Nucl. Phys. A **246**, 395 (1975).

[6] M. Shibata, A. Taniguchi, H. Yamamoto, K. Kawade, J-Z. Ruan, T. Tamai, Y. Kawase, and K. Okano, J. Phys. Soc. Jap. **62**, 87 (1993).

[7] R. Roussille, J. A. Pinston, H. Börner, H. R. Koch, and D. Heck, Nucl. Phys. A **246**, 380 (1975).

[8] R. Roussille, J. A. Pinston, F. Braumandl, P. Jeuch, J. Larysz, W. Mampe, and K. Schreckenbach, Nucl. Phys. A **258**, 257 (1976).

[9] O. Straume and D. G. Burke, Can. J. Phys. C **55**, 1687 (1977).

[10] E. Hammarén, E. Liukkonen, R. Katajanheimo, and T. Tuurnala, Nucl. Phys. A **339**, 465 (1980).

[11] G. Løvhøiden, J. R. Lien, S. El-Kazzaz, J. Rekstad, C. Ellegaard, J. H. Bjerregaard, P. Knudsen, and P. Kleinheinz, Nucl. Phys. A **339**, 477 (1980).

[12] M. Jaskóła, Acta Phys. Pol. B **13**, 63 (1982).

[13] Ts. Venkova, M.-G. Porquet, A. Astier, I. Deloncle, P. Petkov, A. Prévost, F. Azaiez, A. Bogachev, A. Buta, D. Curien, O. Dorvaux, G. Duchêne, J. Durell, B. J. P. Gall, M. Houry, F. Khalfallah, R. Lucas, M. Meyer, I. Piqueras, N. Redon, A. Roach, M. Rousseau, O. Stézowski, and Ch. Theisen, Eur. Phys. J. A **26**, 315 (2005).

[14] N. Nica, Nucl. Data Sheets **110**, 749 (2009).

[15] H. Mach, R. L. Gil, and M. Moszyński, Nucl. Instrum. Methods Phys. Res. A **280**, 49 (1989).

[16] M. Moszyński and H. Mach, Nucl. Instrum. Methods Phys. Res. A **277**, 407 (1989).

[17] H. Mach, F. K. Wohn, G. Molnár, K. Sistemich, John C. Hill, M. Moszyński, R. L. Gill, W. Krips, and D. S. Brenner, Nucl. Phys. A **523**, 197 (1991).

[18] B. Fogelberg, M. Hellström, L. Jacobsson, D. Jerrestam, L. Spanier, and G. Rudstam, Nucl. Instrum. Methods Phys. Res. B **70**, 137 (1992).

[19] R. C. Greenwood, R. G. Helmer, M. H. Putnam, and K. D. Watts, Nucl. Instrum. Methods Phys. Res. A **390**, 95 (1997).

[20] A. J. Aas, H. Mach, M. J. G. Borge, B. Fogelberg, I. S. Grant, K. Gulda, E. Hagebø, W. Kurcewicz, J. Kvasil, A. Lindroth, T. Martinez, D. Nosek, B. Rubio, J. F. Smith, K. Steffensen, I. L. Tain, O. Tengblad, and T. F. Thorsteinsen, Nucl. Phys. A. **611**, 281 (1996).

[21] W. Kurcewicz, I. S. Grant, K. Gulda, A. J. Aas, J. Billowes, M. J. G. Borge, D. G Burke, P. A. Butler, J. F. C. Cocks, B. Fogelberg, S. J. Freeman, G. D. Jones, E. Hagebø, P. Hoff, J. Hønsi, A. Lindroth, G. Løvhøiden, H. Mach, T. Martinez, R. A. Naumann K. Nybø, G. Nyman, H. Ravn, B. Rubio, J. Simpson, A. G. Smith, J. F. Smith, K. Steffensen, I. L. Tain, O. Tengblad, T. F. Thorsteinsen (ISOLDE Collaboration), Nucl. Phys. A. **621**, 827 (1997).

[22] A. J. Aas, Thesis, University of Oslo, Oslo, 1999.

[23] A. J. Aas, H. Mach, J. Kvasil, M. J. G. Borge, B. Fogelberg, I. S. Grant, K. Gulda, E. Hagebø, P. Hoff, W. Kurcewicz, A. Lindroth, G. Løvhøiden, A. Mackova, T. Martinez, B. Rubio, M. Sanchez-Vega, J. F. Smith, I. L. Tain, R. B. E. Taylor, O. Tengblad, T. F. Thorsteinsen (ISOLDE Collaboration), Nucl. Phys. A. **654**, 499 (1999).

[24] L. M. Fraile, A. J. Aas, M. J. G. Borge, B. Fogelberg, L. M. Garcia-Raffi, I. S. Grant, K. Gulda, E. Hagebø, W. Kurcewicz, J. Kvasil, G. Løvhøiden, H. Mach, A. Mackova, T. Martinez, B. Rubio, I. L. Tain, A. G. Teijeiro, O. Tengblad, T. F. Thorsteinsen (ISOLDE Collaboration), Nucl. Phys. A **657**, 355 (1999).

[25] L. M. Fraile, M. J. G. Borge, H. Mach, R. Boutami, A. J. Aas, B. Fogelberg, L. M. Garcia-Raffi, I. S. Grant, K. Gulda, E. Hagebø, W. Kurcewicz, J. Kvasil, M. J. López, G. Løvhøiden, T. Martinez, B. Rubio, I. L. Tain, and O. Tengblad, Nucl. Phys. A. **686**, 71 (2001).

[26] E. Ruchowska, W. A. Płóciennik, J. Żylicz, H. Mach, J. Kvasil, A. Algora, N. Amzal, T. Bäck, M. G. Borge, R. Boutami, P. A. Butler, J. Cederkäll, B. Cederwall, B. Fogelberg, L. M. Fraile, H. O. U. Fynbo, E. Hagebø, P. Hoff, H. Gausemel, A. Jungclaus, R. Kaczarowski, A. Kerek, W. Kurcewicz, K. Lagergren, E. Nacher, B. Rubio, A. Syntfeld, O. Tengblad, A. A. Wasilewski, and L. Weissman, Phys. Rev. C **73**, 044326 (2006).

[27] I. M. Band, M. B. Trzhaskovskaya, C. W. Nestor, P. O. Tikkanen, and S. Raman, At. Data Nucl. Data Tables. **81**, 1 (2002).

[28] G. Alaga, K. Alder, A. Bohr, and B. R. Mottelson, Mat. Fys. Medd. Dan. Vid. Selsk. **29**, 9 (1955).

[29] A. Syntfeld, H. Mach, W. Kurcewicz, B. Fogelberg, W. Płóciennik, and E. Ruchowska, Phys. Rev. C **68**, 024304 (2003).

[30] T. Rząca-Urban, W. Urban, J. A. Pinston, G. S. Simpson, A. G. Smith, and I. Ahmad, Phys. Rev. C **86**, 044324 (2012).

[31] T. Rząca-Urban, W. Urban, A. G. Smith, I. Ahmad, and A. Syntfeld-Każuch, Phys. Rev. C **87**, 031305(R) (2013).

[32] H. J. Li, S. J. Zhu, J. H. Hamilton, E. H. Wang, A. V. Ramayya, Y. J. Chen, J. K. Hwang, J. Ranger, S. H. Liu, Z. G. Xiao, Y. Huang, Z. Zhang, Y. X. Luo, J. O. Rasmussen, I. Y. Lee, G. M. Ter-Akopian, Yu. Ts. Oganessian, and W. C. Ma, Phys. Rev. C **90**, 047303 (2014).

[33] L. K. Peker and J. Tuli, Nucl. Data Sheets **82**, 187 (1997).

[34] N. Nica, Nucl. Data Sheets **117**, 1 (2014).

[35] H. J. Krappe, J. R. Nix, and A. J. Sierk, Phys. Rev. C **20**, 992 (1979).

[36] I. Muntian, Z. Patyk, and A. Sobiczewski, Acta Phys. Pol. B **32**, 691 (2001).

[37] S. Ćwiok, J. Dudek, W. Nazarewicz, J. Skalski, and T. Werner, Comput. Phys. Commun. **46**, 379 (1987).

[38] J. Dudek, Z. Szymański, and T. Werner, Phys. Rev. C **23**, 920 (1981).

[39] P. Jachimowicz, M. Kowal, and J. Skalski, Phys. Rev. C **89**, 024304 (2014).

[40] A. Bohr and B. R. Mottelson, *Nuclear Structure*, Vol. 2 (Benjamin, New York, 1975).

[41] M. Kowal and J. Skalski, Phys. Rev. C **82**, 054303 (2010).

[42] G. A. Leander, W. Nazarewicz, G. F. Bertsch, and J. Dudek, Nucl. Phys. A **453**, 58 (1986).

[43] C. O. Dorso, W. D. Myers, and W. J. Swiatecki, Nucl. Phys. A **451**, 189 (1986).

[44] J. Skalski, Phys. Rev. C **49**, 2011 (1994).